

Mixed convection blowoff limits as a function of oxygen concentration and upward forced stretch rate for burning pmma rods of various sizes

Jeremy W. Marcum[1]
Purdue University, West Lafayette, IN 47907-2040

Paul V. Ferkul[2]
USRA, Cleveland, OH 44135

and

Sandra L. Olson[3]
NASA Glenn Research Center, Cleveland, OH 44135

Normal gravity flame blowoff limits in an axisymmetric pmma rod geometry in upward axial stagnation flow are compared with microgravity Burning and Suppression of Solids – II (BASS-II) results recently obtained aboard the International Space Station. This testing utilized the same BASS-II concurrent rod geometry, but with the addition of normal gravity buoyant flow. Cast polymethylmethacrylate (pmma) rods of diameters ranging from 0.635 cm to 3.81 cm were burned at oxygen concentrations ranging from 14 to 18% by volume. The forced flow velocity where blowoff occurred was determined for each rod size and oxygen concentration. These blowoff limits compare favorably with the BASS-II results when the buoyant stretch is included and the flow is corrected by considering the blockage factor of the fuel. From these results, the normal gravity blowoff boundary for this axisymmetric rod geometry is determined to be linear, with oxygen concentration directly proportional to flow speed. We describe a new normal gravity 'upward flame spread test' method which extrapolates the linear blowoff boundary to the zero stretch limit to resolve microgravity flammability limits—something current methods cannot do. This new test method can improve spacecraft fire safety for future exploration missions by providing a tractable way to obtain good estimates of material flammability in low gravity.

Nomenclature

a stretch rate (s^{-1})
A area (cm^2)
B blockage factor, Eq. 3, Table 1
g gravity (cm/s^2)
K constant, Eq. 5
r radius (cm)
U velocity (cm/s)

Greek
α thermal diffusivity (cm2/s)
δ gas phase length scale (cm)

Subscripts
accel accelerated
b buoyant
o base size
r rod
tube tube

[1] Graduate Student, Aerospace Engineering, Purdue University, West Lafayette, IN.
[2] Spacecraft Fire Safety Scientist, USRA, NASA Glenn Research Center, Cleveland, OH.
[3] Spacecraft Fire Safety Scientist, NASA Glenn Research Center, Cleveland, OH.

I. Introduction

DIFFUSION flames in stagnation flow have long been studied due to their ease of control, amenability to diagnostic measurement and modeling, and reproducibility of results. Early work [1] on flammability limits has demonstrated that a hemispherical stagnation flow geometry is a reliable method to obtain the flammability limits of various fuels as a function of upward flowing oxidizer gas. Many heavier hydrocarbons were found to have similar limiting oxygen concentrations (13%-14%) and flame temperatures (1450-1500°C). Spalding [2] used the spherical stagnation geometry to help define his Transfer Number versus critical stretch rate U/2r for extinction. Tsuji and coworkers utilized the 2D stagnation geometry for many years to quantify both diffusion flames and premixed flame structure and extinction limits [3, 4].

Linan [5] utilized the stagnation geometry to develop his large activation energy asymptotic analysis for steady flame structure and derivation of a critical Damkohler number for extinction. Sohrab et al. [6] expanded Linan's asymptotic work on extinction limits to include gas-phase radiant loss. Krishnamurthy [7] experimentally studied pmma rod tip blowoff at various oxygen and pressure ambient atmospheres and applied the critical Damkohler number for extinction [5].

T'ien and coworkers [8-9] have developed detailed numerical models of stagnation flames over solid surfaces, including surface radiation, and subsequently gas phase radiation as well [10, 11]. The models were used to outline a complete flammability boundary in terms of oxygen and forced stretch rate. Some experiments with pmma rods [12] outlined a similar flammability boundary.

Recent testing completed on the International Space Station investigated the oxygen-flow flammability boundary for three different cast PMMA rod sizes [13]. This paper describes normal gravity forced flow blowoff tests conducted to complement these flight results.

II. Experiment Description

The test setup depicted in Fig. 1 was used to determine the blowoff limits for cast PMMA rods having different radii. Five radii of cast clear PMMA rods were tested; 0.318 cm, 0.476 cm, 0.635 cm, 1.270 cm, and 1.905 cm, spanning a factor of six in radius. The apparatus consists of a flow system with two sources of gas; shop air and calibrated premixed bottles of 14% to 18% oxygen by volume in balance nitrogen. A manual valve is used to switch the gas source. The gas flows through a 200 SLPM MKS mass flow controller and into a flow straightener, which provides a uniform exiting flow profile, verified by hot wire anemometer profiling. The flow then enters the quartz tube, which has a 7.6 cm inside diameter (nearly identical in size to the LOI test standard tube size [14]) and is 25.4 cm long. Matte black foil eliminates reflections from the back of the tube. A color video camera records each experiment through the clear tube. An exhaust snorkel above the tube removes combustion products from the lab.

Each experiment begins by imaging a scale inside the tube next to the rod along with a card noting the test conditions. Shop air dried using an O'Keefe air dryer is set to the desired test flow rate on the mass flow controller. Each of the cast PMMA rods, hanging from a metal crossbar, was ignited with a small lighter outside of the apparatus and then suspended in the flow tube. Each initially flat-ended rod was allowed to burn to a rounded tip which is more representative of the steady-state shape of a burning sample.

Once the flame stabilized inside the tube, the gas source was switched from dry shop air to the premixed bottle test gas at the same flow rate to determine if the flame would blow off at that flow and oxygen combination. The lowest flow rate where blowoff occurs was determined iteratively for each oxygen concentration. Due to limitations in system pressures, the maximum flow rate was 165 SLPM (60.3 cm/s average tube speed). This limited the range of oxygen concentrations where blowoff could be obtained.

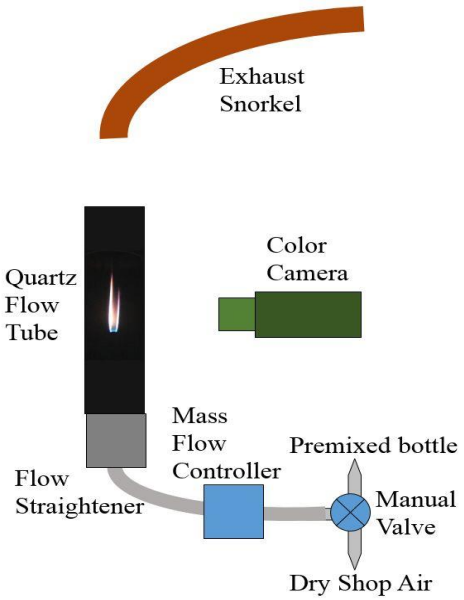

Fig. 1. Test apparatus schematic used for blowoff testing.

III. Results

Over 280 experiments were conducted to determine the blowoff limits for each oxygen concentration and rod radius, and the bracketing flow conditions were repeated at least once. From the test images, some general trends are noted. Flame blowoff always occurs at the stagnation region. The triggering event appears to be the development of a flame hole [15] at the stagnation region of sufficient size to destabilize the flame base. Small flame holes might disappear or be "healed," but a subsequent larger hole can destabilize the flame and lead to blowoff.

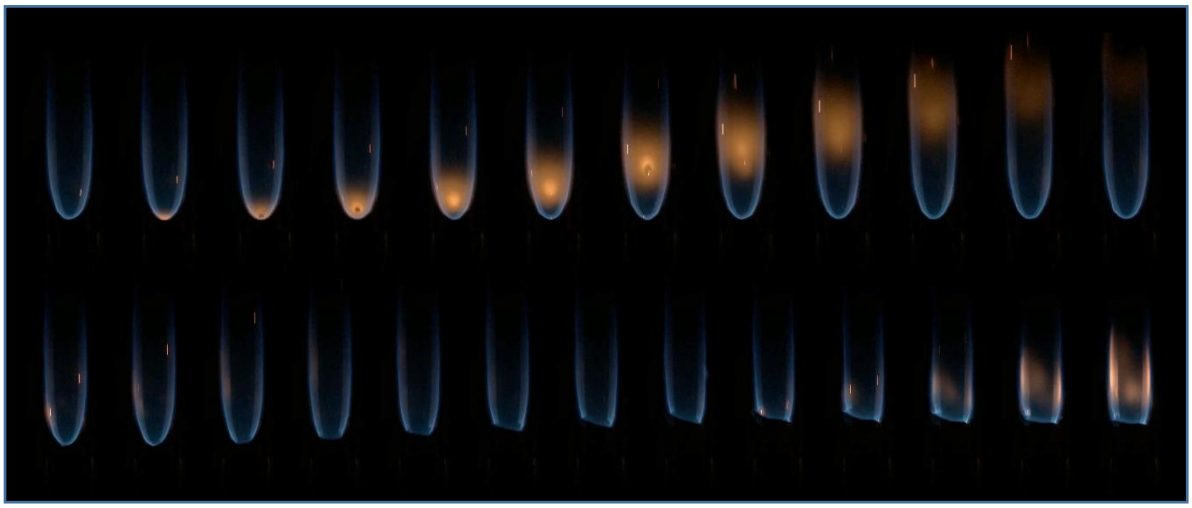

Fig. 2. Sequence of 16% O_2 by volume flame images showing top: a small stagnation hole that heals and bottom: a hole that causes blowoff.

This is shown in Fig. 2. In the top sequence of images (at 120 f/s), a small hole forms at the stagnation region, and moves up the side of the flame. The stagnation region heals, but the hole persists for a number of frames as it is convected up the side of the flame. A sooty region forms around the hole. It may be that a vapor jet from a bubble rupture from the surface is the triggering event. The vapor jet increases the local strain rate, causing local flame extinction. The excess fuel from the jet exits the flame sheet and creates a locally fuel rich region outside the hole which then reacts, causing the sooty region.

In the bottom sequence of images (at 80 f/s) from later in the same test and under the same test conditions, a small hole again forms but quickly grows to the scale of the 0.476 cm rod diameter. The stagnation region destabilizes. Due to the destabilization, the flame quickly blows downstream. The sequence ends as the flame develops a bright blue flame base that anchors briefly to the sides of the cylinder. The downstream section of the flame becomes sooty, which seems to correspond with the formation of the anchor ring (flame base of the side-stabilized flame). This ring is interpreted as the outer lip of the triple flame at the flame leading edge.

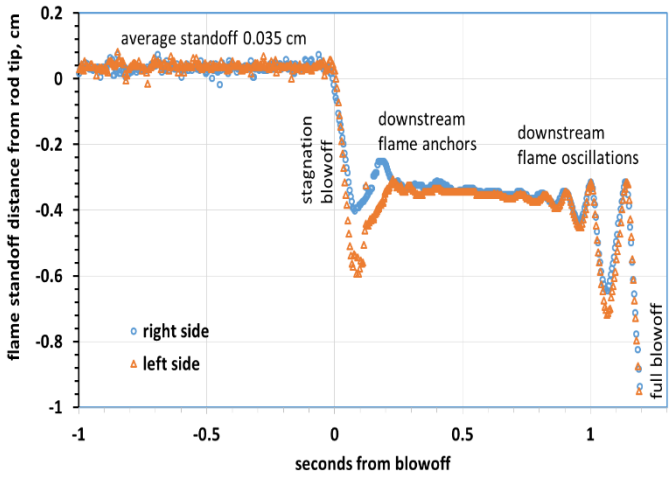

Fig. 3. Flame hole edge positions during blowoff

The positions of the left and right sides of the flame hole during the lower blowoff sequence are tracked in Fig. 3 with time. The flame is initially stabilized less than 1 mm below the rod. Once the hole forms (set to be time zero), the flame quickly moves downstream. The right side of the flame anchors at -0.4 cm and the left side at -0.6 cm, and the anchor ring starts to move back upstream. The anchor ring then settles at approximately -0.35 mm for over half a second. The anchor ring then begins to oscillate up and down with increasing amplitude until the side-stabilized flame blows off completely. The side stabilized flame at oxygen concentrations less than the downward Limiting Oxygen Index (LOI) is not expected to be stable.

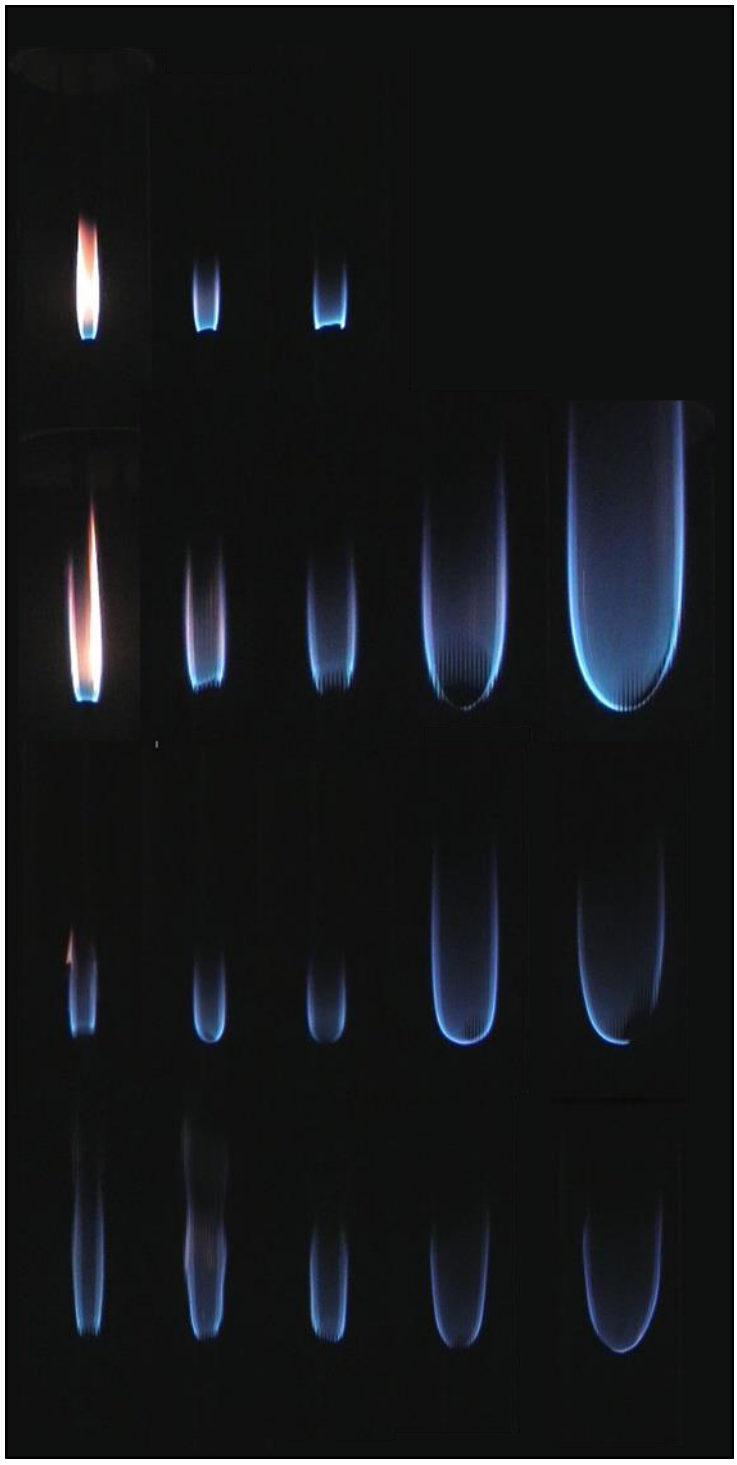

Fig. 4. Flame images just before blowoff for each oxygen concentration and rod radius.

Figure 4 shows the flames just as blowoff begins at each limiting flow condition. Note that at 18% oxygen, blowoff limits are found at only three radii due to flow rate limitations. Most of the flames at blowoff are primarily blue, but more sooting is observed for the smallest rod radii and higher oxygen concentrations. The larger the radius, the larger the flame hole needs to be to destabilize the flame, which is consistent with [15] for flame holes in the presence of a heat sink.

Figure 5 presents the blowoff boundaries found for each rod radius in terms of oxygen concentration versus forced flow velocity. Each boundary is approximately linear with flow, with the exception of the 14% oxygen data, where all the data collapses at forced flow velocities less than 5 cm/s. This result is anomalous and explained as follows. At a sufficiently low forced flow rate, entrainment of air into the quartz tube from the top might be mixing with the supplied gas, increasing the ambient oxygen concentration so that the rod remains flammable.

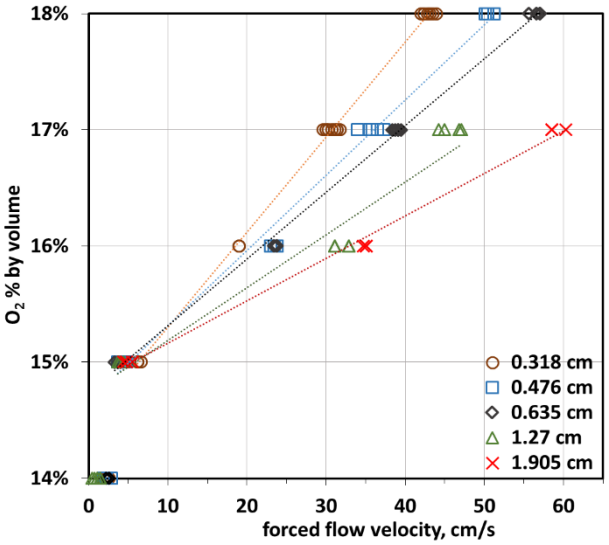

Fig. 5. Blowoff boundaries for each rod radius as a function of oxygen concentration and forced flow velocity

To investigate this behavior, tests were repeated in the larger ZGRF wind tunnel rig [16] at the same normal gravity conditions of 14% O_2 and 2 cm/s flow. The wind tunnel rig provides a 20 cm diameter flow system with much less chance of entraining air from the top. Unlike in the 1g setup in the lab, the rod blew off in repeated tests at 14% oxygen in the larger wind tunnel as shown in Fig. 6. A test was then repeated at 15% O_2 in the ZGRF wind tunnel to determine whether there was still an entrainment effect in the quartz tube data at the higher flow speeds. However, this flame did not blow off. Given these results, the 14% O_2 data are discarded from further analysis.

Fig.6 Non-symmetric flame in quartz tube at 14% oxygen, left, does not blowoff due to ambient flow entrainment back into the tube. Flame does blow off in larger wind tunnel, right, at 14% oxygen and 2 cm/s forced flow. Note: camera systems are not the same, although images are approximately to scale.

Figure 7 plots the blowoff forced stretch rate as a function of rod radius r for each oxygen concentration. The forced stretch rate is defined as a=3/2 U/r, where U is the average flow speed entering the tube and r is the rod radius. The data at each oxygen concentration is fitted with a power law having a square root exponent, which is attributed to the flame stretch at the flame standoff distance rather than the rod surface. The flame standoff distance is estimated using the gas phase thermal length scale, defined as

$$\delta = (\alpha/a)^{1/2} \qquad \text{Eq.(1)}$$

where α is the gas phase thermal diffusivity and a is the stretch rate defined above. This length scale δ is thus proportional to $r^{1/2}$ for a given velocity U. In the inset, the coefficient C for each power law fit is plotted versus oxygen, revealing that the forced stretch rate at blowoff varies linearly with oxygen in addition to varying as the square root of the rod radius. These relationships guided the subsequent correlation of the data.

To collapse the data at different radii into a single blowoff boundary, the flame curvature needs to be accounted for, so for a given flow speed we introduce the normalized thermal length ratio $\delta/\delta_o = (r/r_o)^{1/2}$ discussed above where r_o is the smallest rod radius = 0.318 cm. In addition, the flow acceleration in the quartz tube due to the presence of the rod becomes significant for the larger rod sizes, as noted by [4]. To account for this flow acceleration, a blockage factor was defined as $B=A_{tube}/(A_{tube}-A_r)$ as follows:

$$U_{tube}\,A_{tube} = U_{accel}\,(A_{tube} - A_r) \quad \text{Eq. (2)}$$

$$U_{accel} = \frac{U_{tube}\,A_{tube}}{(A_{tube} - A_r)} = BU_{tube} \quad \text{Eq. (3)}$$

Where U_{tube} = U in the stretch rate definition, and A_{tube} and A_r are the cross-sectional areas of the tube and rod, respectively. Table 1 shows the B values for each r.

Table 1: Blockage factor B for each rod radii

r, cm	A_r, cm^2	A_{tube}, cm^2	B
0.318	0.318	45.604	1.007
0.476	0.712	45.604	1.016
0.635	1.267	45.604	1.029
1.270	5.067	45.604	1.125
1.905	11.401	45.604	1.333

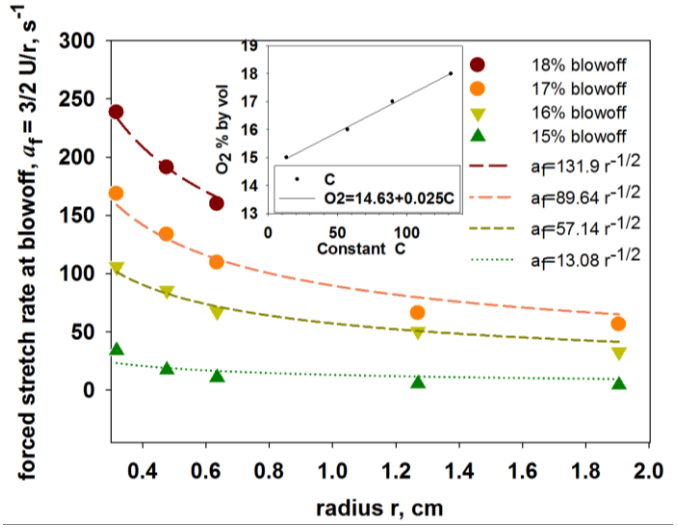

Fig. 7. Forced stretch rate at blowoff plotted against rod radius at each oxygen concentration. The inset shows the constant of each power law curve fit, which varies linearly with oxygen.

Using these corrections, an adjusted forced stretch rate a_o is defined as

$$a_o = \left[\frac{3}{2}\frac{U}{r}\right] * \left[\frac{A_{tube}}{(A_{tube} - A_r)}\right] * \left[\frac{r}{r_o}\right]^{1/2} \quad (4)$$

The blowoff data from Fig. 5 and Fig. 7 is replotted using the adjusted forced stretch rate as the x-axis in Fig. 8. The data collapses into a single blowoff boundary for all the normal gravity data. The BASS-II flammability boundary [13] is also plotted in Fig. 8. There is a clear offset between the normal gravity data and the microgravity data. An empirical linear superposition of the buoyant stretch rate of a_b=80 s^{-1} is used to align the data with the BASS-II boundary ($a_{total} = a_o + a_b$). For the smallest rod size, this is an effective forced flow of 17 cm/s, in good agreement with normal gravity buoyant flow velocities (~ 20 cm/s) [17]. The linear fit to the shifted data is given by the blue-shaded band. This blowoff region is inherently wide due to the stochastic nature [18] of the blowoff limit.

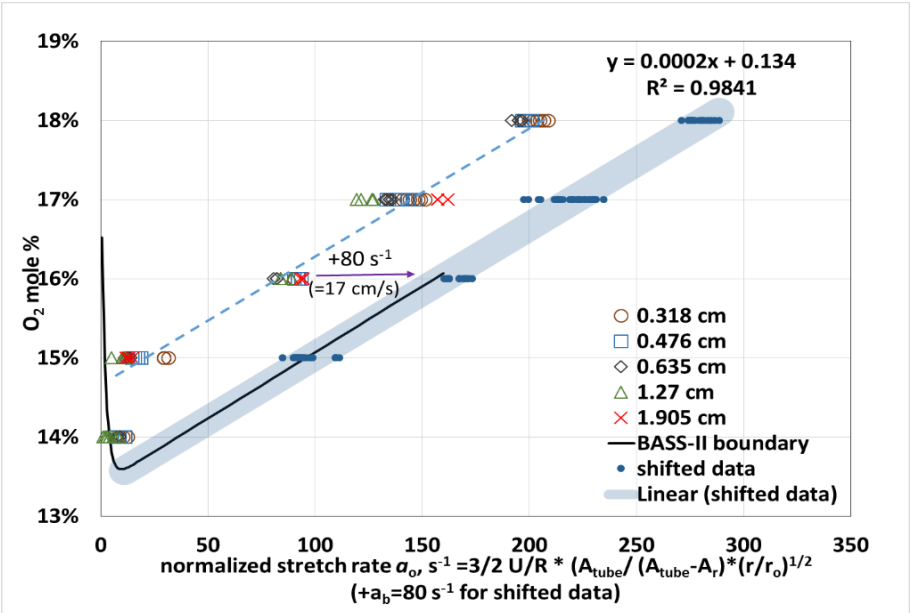

Fig. 8. Blowoff boundary correlation that accounts for the flow acceleration due to rod blockage in the quartz tube, and normalizes all the radii to the smallest radius r_o using the gas phase length scale δ. To account for buoyant stretch, a shift of 80 s^{-1} aligns the normal gravity data with BASS-II data [13]

To check this correlation with previous experiments, the blowoff data from Halli and T'ien [12] is plotted in Fig. 9 using the same buoyant flow shift for their rod radius of 0.635 cm. It is seen that the blowoff branch data shifts into the BASS-II boundary for most of the blowoff branch (a>~a_b)

The linear trend in blowoff data with oxygen is noteworthy and potentially useful for developing an improved test method that can be performed in normal gravity to determine flammability in microgravity. The idea is that the actual flammability boundary as given by the BASS-II data can be approximated simply by the extrapolating the linear blowoff boundary to zero stretch, which estimates that 13.4% O_2 is the limiting oxygen concentration below which the fuel cannot burn at any stretch rate. From a fire safety perspective, it is a conservative estimate but still quite close to the observed 13.6% O_2 minimum concentration needed to get stable flames in BASS-II [12]. The estimate is good because the microgravity quenching boundary turns upward away from the blowoff line only for very low-speed flows, a very narrow region compared to the overall boundary.

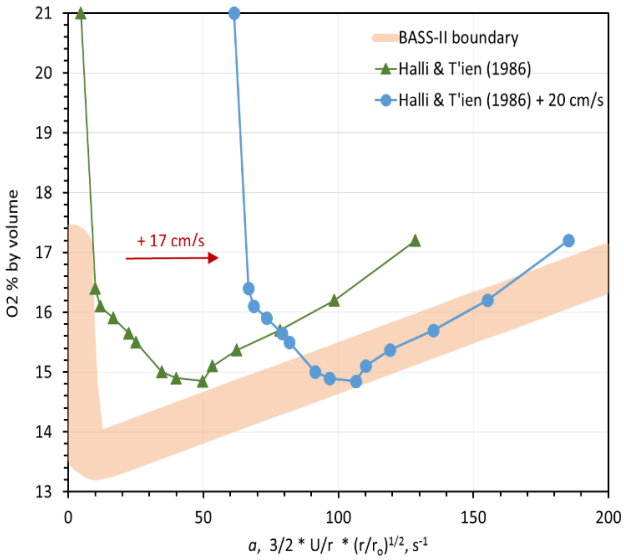

Fig. 9. Data from Halli & T'ien [12] shifted to account for buoyant stretch compared to the BASS-II boundary.

The use of an empirical shift to determine the buoyant stretch predicates knowledge of the microgravity boundary, which is not generally the case. Using another way to account for the shift, consider the formulation from [19] where the buoyant stretch takes the form

$$a_b = K\sqrt{\frac{g}{r}} \tag{5}$$

Using values a_b = 80 s^{-1}, g=981 cm/s^2, and r_o = 0.318 cm, the constant K in Eq. 5 is estimated to be 1.44. Further research is needed to determine the applicability of the buoyant stretch constant K for different materials. Since K is a density ratio [19], and gas-phase chemistry at the blowoff limit may have the same limiting reaction rate for a given flow rate (critical Damkohler number), the critical temperatures may be similar for different materials with the same basic gas phase chemistry [1] at each oxygen concentration. Thus for common C-H-O fuels one would expect the density ratio to also be similar at blowoff. Differences in flammability limits may be attributed to differences in solid phase degradation kinetics [20]. On the other hand, fuels with other chemical additives (N, Br, Cl, P, etc.) that impact the gas phase chemistry may not follow the same trends to complement these flight results.

IV. Conclusions

Normal gravity blowoff limits were measured for the axisymmetric cast PMMA rod geometry in upward axial stagnation flow. Five radii (0.318 cm to 1.905 cm) at five oxygen concentrations (14 to 18% by volume) were tested. The blowoff velocities were converted to forced stretch rates. By using a normalized thermal length ratio $\delta/\delta_o = (r/r_o)^{1/2}$ to account for the stretch rate at the flame standoff distance and normalizing the results to the base rod size as well as adjusting the flow due to rod blockage in the tube, all the data was correlated onto a single curve.

The blowoff boundary in normal gravity was compared to the complete microgravity extinction boundary from the Burning and Suppression of Solids – II (BASS-II) experiments performed aboard the International Space Station. The normal gravity blowoff boundary was parallel to the BASS-II boundary, but shifted to lower stretch rates. To account for the additional inherent buoyant stretch, the normal gravity boundary was empirically shifted to the right by a value a_b =80 s^{-1}, which for the base rod size corresponds to a forced flow velocity of 17 cm/s, in good agreement with buoyant flow velocity estimates.

We suggest an improved normal gravity 'upward flame spread test' method to estimate material flammability in microgravity. The first step is to determine the normal gravity blowoff boundary for an axisymmetric rod geometry burning in a forced flow tube. Then, the buoyant stretch contribution is corrected for to predict the microgravity

blowoff boundary. Further research is needed to determine the applicability of the buoyant stretch constant K for different materials. If proven for various C-H-O materials, this linear boundary, extrapolated to zero stretch, could provide a conservative estimate of flammability limits in microgravity. The technique may work for a wide range of materials as long as the gas-phase chemistry is similar. This test method may improve spacecraft fire safety for future exploration missions.

Acknowledgments

The ISS Research Project Office funded this work. The authors want to acknowledge the personnel from the NASA Glenn Zero Gravity Research Facility, led by Professional Engineer Eric Neumann, for their assistance in preparation of the rod samples, design and fabrication of the flow straightener and flow system, and support of supplemental wind tunnel normal gravity testing at 14% oxygen. The authors would also like to thank Jay Owens for his help in setting up the camera control system for normal gravity testing.

References

[1] Simmons, R.F. and Wolfhard, H.G., 1957. Some limiting oxygen concentrations for diffusion flames in air diluted with nitrogen. *Combustion and Flame, 1*(2), pp.155-161. http://dx.doi.org/10.1016/0010-2180(57)90042-1

[2] Spalding, D.B., 1953, December. The combustion of liquid fuels. In *Symposium (international) on combustion* (Vol. 4, No. 1, pp. 847-864). Elsevier.

[3] Tsuji, H., 1982. Counterflow diffusion flames. Progress in energy and combustion science, 8(2), pp.93-119. http://dx.doi.org/10.1016/0360-1285(82)90015-6

[4] Tsuji, H. and Yamaoka, I., 1967, December. The counterflow diffusion flame in the forward stagnation region of a porous cylinder. In Symposium (International) on Combustion (Vol. 11, No. 1, pp. 979-984). Elsevier. http://dx.doi.org/10.1016/s0082-0784(67)80224-8

[5] Linan, A., 1974. The asymptotic structure of counterflow diffusion flames for large activation energies. *Acta Astronautica*, *1*(7-8), pp.1007-1039. http://dx.doi.org/10.1016/0094-5765(74)90066-6

[6] Sohrab, S.H., Linan, A. and Williams, F.A., 1982. Asymptotic theory of diffusion-flame extinction with radiant loss from the flame zone. *Combustion Science and Technology*, *27*(3-4), pp.143-154. http://dx.doi.org/10.1080/00102208208946983

[7] Krishnamurthy, L., 1975. Diffusion-flame extinction in the stagnation-point boundary layer of PMMA in O2/N2 mixtures. Combustion science and technology, 10(1-2), pp.21-25. http://dx.doi.org/10.1080/00102207508946654

[8] T'ien, J.S., 1986. Diffusion flame extinction at small stretch rates: the mechanism of radiative loss. *Combustion and Flame*, *65*(1), pp.31-34. http://dx.doi.org/10.1016/0010-2180(86)90069-6

[9] T'ien, J.S. and Foutch, D.W., 1987. Extinction of a stagnation-point diffusion flame at reduced gravity. AIAA journal, 25(7), pp.972-976.

[10] Rhatigan, J.L., Bedir, H. and James, S., 1998. Gas-phase radiative effects on the burning and extinction of a solid fuel. *Combustion and Flame*, *112*(1), pp.231-241. doi:10.1016/S0010-2180(97)81771-3

[11] T'ien, J.S., 2008. Some Partial Scaling Considerations in Microgravity Combustion Problems. Progress in Scale Modeling, pp.281-292. http://dx.doi.org/10.1007/978-1-4020-8682-3

[12] Halli, Y., T'ien, J.S., NBS-GCR-86-507 (1986).

[13] Olson, S.L. and Ferkul, P.V., Microgravity Flammability Boundary for PMMA Rods In Axial Stagnation Flow: Results of the ISS BASS-II Experiments, 9th U. S. National Combustion Meeting, The Combustion Institute, May 17-20, 2015, Cincinnati, Ohio, submitted to Combustion and Flame.

[14] ASTM, D., 2010. 2863-10, Standard Test Method for Measuring the Minimum Oxygen Concentration to Support Candlelike Combustion of Plastics (oxygen index). ASTM Int, West Conshohocken, PA.

[15] Nayagam, V., Balasubramaniam, R. and Ronney, P.D., 1999. Diffusion flame-holes. Combustion theory and modelling, 3(4), pp.727-742. http://dx.doi.org/10.1088/1364-7830/3/4/307

[16] Olson, S.L. and Miller, F.J., 2009. Experimental comparison of opposed and concurrent flame spread in a forced convective microgravity environment. Proceedings of the Combustion Institute, 32(2), pp.2445-2452. http://dx.doi.org/10.1016/j.proci.2008.05.081

[17] Hirano, T., Noreikis, S.E. and Waterman, T.E., 1974. Measured velocity and temperature profiles near flames spreading over a thin combustible solid. *Combustion and Flame*, *23*(1), pp.83-96. doi:10.1016/S0010-2180(74)80029-5

[18] T'ien, J.S., 1973. The Effects of Perturbations on the Flammability Limits. Combustion Science and Technology, 7(4), pp.185-188. http://dx.doi.org/10.1080/00102207308952357

[19] Olson, S.L. and T'ien, J.S., 2000. Buoyant low-stretch diffusion flames beneath cylindrical PMMA samples. Combustion and Flame, 121(3), pp.439-452. http://dx.doi.org/10.1016/S0010-2180(99)00161-3

[20] Walters, R.N. and Lyon, R.E., 2003. Molar group contributions to polymer flammability. *Journal of Applied Polymer Science*, *87*(3), pp.548-563. http://dx.doi.org/10.1002/app.11466